Electronic-nuclear entanglement in H_2^+: Schmidt decomposition of non-Born-Oppenheimer wave functions expanded in nonorthogonal basis sets

José Luis Sanz-Vicario,[1,*] Jhon Fredy Pérez-Torres,[2,†] and Germán Moreno-Polo[1]
[1]*Grupo de Física Atómica y Molecular, Instituto de Física, Universidad de Antioquia, Medellín, Colombia*
[2]*Facultad de Ciencias Básicas. Universidad de Medellín, Medellín, Colombia*
(Received 10 June 2017; published 2 August 2017)

We compute the entanglement between the electronic and vibrational motions in the simplest molecular system, the hydrogen molecular ion, considering the molecule as a bipartite system, electron and vibrational motion. For that purpose we compute an accurate total non-Born-Oppenheimer wave function in terms of a huge expansion using nonorthogonal *B*-spline basis sets that expand separately the electronic and nuclear wave functions. According to the Schmidt decomposition theorem for bipartite systems, widely used in quantum-information theory, it is possible to find a much shorter but equivalent expansion in terms of the natural orbitals or Schmidt bases for the electronic and nuclear half spaces. Here we extend the Schmidt decomposition theorem to the case in which nonorthogonal bases are used to span the partitioned Hilbert spaces. This extension is first illustrated with two simple coupled systems, the former without an exact solution and the latter exactly solvable. In these model systems of distinguishable coupled particles it is shown that the entanglement content does not increase monotonically with the excitation energy, but only within the manifold of states that belong to an existing excitation mode, if any. In the hydrogen molecular ion the entanglement content for each non-Born-Oppenheimer vibronic state is quantified through the von Neumann and linear entropies and we show that entanglement serves as a witness to distinguish vibronic states related to different Born-Oppenheimer molecular energy curves or electronic excitation modes.

DOI: 10.1103/PhysRevA.96.022503

I. INTRODUCTION

Most quantum chemistry calculations are based on the successful Born-Oppenheimer (BO) approximation for a molecule, which can be thought of as a bipartite coupled system composed of electrons and nuclei according to quantum-information theory [1]. The BO wave function is expressed as a direct product of an electronic wave function (which depends parametrically on the nuclear geometry) times a nuclear wave function. However, such a molecular BO wave function is not a true eigenfunction of the molecular Hamiltonian, since the so-called nonadiabatic coupling terms are missing and with them, some of the intricate features of the correlation between electrons and nuclei.

There has been a rising interest in the understanding of the fundamental entanglement between the electronic and nuclear motion in molecules [2–7]. A proper account of this correlation contributes to the quantification of the electronic-nuclear entanglement beyond the BO approximation. It has been recently pointed out that the BO wave function has already an offset entanglement [4,7] yet to be quantified in a realistic molecular system. In this work we attempt to quantify the full non-BO entanglement between the electronic and nuclear subsystems in the simplest molecule (hydrogen molecular ion H_2^+) by using a variational molecular wave function (pure state) which is a true eigenfunction of the molecular Hamiltonian. This means that all nonadiabatic couplings are intrinsically included in this approach.

Here we employ the Schmidt decomposition theorem [1,8,9], which allows us to calculate the von Neumann and linear entropies as entanglement measures, as well as the Schmidt bases for the electronic and nuclear motions in H_2^+. In order to calculate the non-BO eigenstates of the molecular Hamiltonian of a nonrotating H_2^+ molecular ion, we use a variational configuration interaction (CI) method in which we expand the state in terms of products of *B*-splines [10,11] and Legendre polynomials for the radial and angular part of the electronic motion, respectively, times *B*-spline polynomials for the relative nuclear motion (see [12] for details). Nonorthogonal bases are commonly used in atomic and molecular electronic structure calculations (Slaters, Gaussians, *B*-splines, etc.). However, the standard Schmidt decomposition theorem is formulated in terms of orthonormal bases that span both Hilbert half spaces of the bipartite system, which precludes a direct algebraic use of the theorem with most current atomic and molecular wave functions and basis sets. Although a simple solution could be a pre-orthogonalization of the basis, the computational effort is prohibitive when huge basis sets are in use, as is the case for non-BO wave functions in molecules. Here we propose a practical algebraic extension of the Schmidt decomposition theorem to nonorthogonal bases. Reference [13] is to our knowledge the only reference with a particular use of the Schmidt decomposition theorem and the natural orbitals for the ground state in HD^+, where reduced density matrices are obtained by direct numerical integration. The goal in Ref. [13] was not to evaluate any BO or non-BO entanglement but to assess the performance of a multiconfigurational time-dependent Hartree-Fock method for the combined electronic-nuclear dynamics in diatoms.

To validate our nonorthogonal procedure we start by studying a couple of two-dimensional (2D) model systems, for which we also use a variational CI method. The first consists of two coupled particles confined within a box, without known

*Corresponding author: jose.sanz@udea.edu.co
†Present address: Escuela de Química, Universidad Industrial de Santander, Bucaramanga, Colombia.

exact solution, and the second is a system of two coupled harmonic oscillators, nonseparable and entangled in Cartesian coordinates but with exact solution after a rotation to normal mode coordinates. The latter is thus separable only in a given coordinate system. It is worth noting that the entanglement concept relies on the chosen way of the partitioning of the system into selected subsystems. A particular set of coordinates may bring the state to a separable form within this particular partitioning, for which the state is unentangled, but the same state remains entangled in the rest of the possible partitions. These model systems (with distinguishable particles and without spin) also allow us to analyze the behavior of entanglement with the excitation energy. We show that entanglement in complex multidimensional systems of distinguishable particles does not in general increase monotonically with the excitation energy, as is commonly believed, although if excited states are arranged into approximate excitation modes, the entanglement increases monotonically within each mode. A similar conclusion can be drawn for non-BO $H_2{}^+$, for which entanglement increases within each approximate BO electronic excitation mode.

The paper is organized as follows: In Sec. II we describe the basics related to the Schmidt decomposition theorem in its canonical form using orthonormal basis sets in both half spaces and its practical algebraic application when using variational linear expansions in the form of a CI method. Here we contribute with the extension of the Schmidt decomposition theorem when using nonorthogonal basis set: by applying, first, the well-known Löwdin orthogonalization method that transforms the nonorthogonal expansion coefficients into orthogonal ones and brings the procedure to the Schmidt canonical form and, second, a proper nonorthogonal method that eventually can be used more efficiently for huge variational expansions. In Sec. III we illustrate our approaches with simple toy models: we analyze the entanglement content in two coupled particles within a 2D box and two coupled harmonic oscillators in 2D, with Schmidt half spaces taken in terms of Cartesian coordinates. Finally we present results on the electronic-nuclear entanglement in $H_2{}^+$ by starting with the accurate computation of non-BO eigenstates in terms of nonorthogonal basis sets. We finish with some conclusions and perspectives in Sec. IV. Atomic units (a.u.) are used throughout unless otherwise stated.

II. THEORY

A. Schmidt theorem with orthonormal basis

The Schmidt decomposition theorem (see for instance [1,9]) applies to bipartite systems; i.e., the whole system can be partitioned in two subsystems U and V. The theorem is related to the singular value decomposition in matrix algebra. In principle the specific choice for the half spaces can be quite arbitrary. Suppose we take two sets of orthonormal bases $\{|\tilde{\phi}_i\rangle\}_{i=1}^{M}$ and $\{|\tilde{\chi}_j\rangle\}_{j=1}^{N}$ (throughout the paper we use the tilde notation to indicate the orthogonal case) that span the Hilbert subspaces $\mathcal{H}_U$ and $\mathcal{H}_V$ for the subsystems U and V, respectively. Then the total Hilbert space is a direct sum $\mathcal{H} = \mathcal{H}_U \oplus \mathcal{H}_V$ and any state $|\Psi\rangle \in \mathcal{H}$ can be decomposed in a so called *configuration interaction* (CI) form

$$|\Psi\rangle = \sum_{i,j}^{M,N} \tilde{C}_{ij} |\tilde{\phi}_i, \tilde{\chi}_j\rangle, \tag{1}$$

where $\tilde{C}_{ij}$ are the CI expansion coefficients and $|\tilde{\phi}_i, \tilde{\chi}_j\rangle \equiv |\tilde{\phi}_i\rangle \otimes |\tilde{\chi}_j\rangle$ is a configuration written as a direct product. Accordingly the spectral decomposition of the full density operator $\hat{\rho} = |\Psi\rangle\langle\Psi|$ is

$$\hat{\rho} = \sum_{i,j,k,\ell}^{M,N,M,N} \rho_{ij;kl} |\tilde{\phi}_i \tilde{\chi}_j\rangle\langle\tilde{\phi}_k \tilde{\chi}_\ell|, \tag{2}$$

where the matrix elements are simply built from the expansion coefficients, i.e., $\rho_{ij;k\ell} = \tilde{C}_{ij}\tilde{C}^*_{k\ell}$ (given that the basis vectors are orthogonal). The Schmidt decomposition theorem states that any bipartite pure state admits a much simpler expansion

$$|\Psi\rangle = \sum_{i=1}^{\min(M,N)} \sqrt{\lambda_i} |u_i, v_i\rangle, \tag{3}$$

where $|u_i\rangle$ and $|v_i\rangle$ are the (orthogonal) reduced Schmidt bases, which are eigenstates of the reduced density matrices $\hat{\rho}^u = \mathrm{Tr}_v \hat{\rho}$ and $\hat{\rho}^v = \mathrm{Tr}_u \hat{\rho}$, respectively, and with the same set of eigenvalues λ_i, e.g.,

$$\hat{\rho}^u |u_i\rangle = \lambda_i |u_i\rangle, \quad \hat{\rho}^v |v_i\rangle = \lambda_i |v_i\rangle, \tag{4}$$

where these eigenvalues satisfy $0 \leqslant \lambda_i \leqslant 1$ and $\sum_{i=1}^{\min(M,N)} \lambda_i = 1$. The eigenvalues λ_i with $\min(M,N) < i \leqslant \max(M,N)$ are zero.

In practice, with CI expansions for the total wave function (1) based on orthogonal basis sets, the construction of the matrix representation of the reduced density operators is straightforward, i.e.,

$$\rho^u_{ik} = \sum_{j=1}^{M} \tilde{C}_{ij}\tilde{C}^*_{kj}, \quad \rho^v_{j\ell} = \sum_{i=1}^{N} \tilde{C}_{ij}\tilde{C}^*_{i\ell}. \tag{5}$$

These two matrices $\boldsymbol{\rho}^u$ (with size $M \times M$) and $\boldsymbol{\rho}^v$ (with size $N \times N$) can be diagonalized as typical algebraic eigenvalue problems

$$\boldsymbol{\rho}^u \tilde{\mathbf{c}}^u = \Lambda \tilde{\mathbf{c}}^u, \quad \boldsymbol{\rho}^v \tilde{\mathbf{c}}^v = \Lambda \tilde{\mathbf{c}}^v, \tag{6}$$

and the orthonormal Schmidt basis are their eigenvectors expressed in terms of the original orthonormal basis sets, i.e.,

$$|u_i\rangle = \sum_{m=1}^{M} \tilde{c}^u_{im} |\tilde{\phi}_m\rangle, \quad |v_j\rangle = \sum_{n=1}^{N} \tilde{c}^v_{jn} |\tilde{\chi}_n\rangle. \tag{7}$$

B. Schmidt theorem with nonorthogonal basis sets

1. *Löwdin orthogonalization*

Let us assume that the CI vector $|\Psi\rangle$ in (1) is expanded in a nonorthogonal basis set. To our knowledge there is no extension of the Schmidt theorem when using nonorthogonal basis sets. We can remedy this situation by simply orthogonalizing the basis set. A well-known procedure is the Löwdin symmetric orthogonalization method [14,15]. In this method one looks for a transformation that brings the overlap matrix $\mathbf{S}$ for the basis set to the identity matrix, i.e., $\mathbf{X}^\dagger \mathbf{S} \mathbf{X} = \mathbf{1}$,

and a simple choice is $\mathbf{X} = \mathbf{S}^{-1/2}$. Note that the full overlap matrix $\mathbf{S}$ is built as a Kronecker product of two separated overlap matrices, i.e., $S_{ij;k\ell} = (S^u \otimes S^v)_{ij;k\ell} = S^u_{ik} S^v_{j\ell}$. Then the nonorthogonal basis sets $\{|\phi_i\rangle\}$ and $\{|\chi_i\rangle\}$ corresponding to the Hilbert spaces $\mathcal{H}_U$ and $\mathcal{H}_V$, respectively, can be orthonormalized separately to obtain the new sets $\{|\tilde{\phi}_i\rangle\}$ and $\{|\tilde{\chi}_j\rangle\}$ as follows:

$$|\tilde{\phi}_i\rangle = \sum_{m=1}^{M} (S^u)^{-1/2}_{mi} |\phi_m\rangle, \quad |\tilde{\chi}_j\rangle = \sum_{n=1}^{N} (S^v)^{-1/2}_{nj} |\chi_n\rangle. \tag{8}$$

Accordingly, the CI expansion coefficients C_{ij} (now in terms of nonorthogonal basis sets) can be straightforwardly transformed into orthogonal expansion coefficients for the new orthogonal basis (8) with a simple matrix-vector multiplication

$$\tilde{C}_{ij} = \sum_{mn} (S^{1/2})_{ij;mn} C_{mn}, \quad \tilde{C}^*_{k\ell} = \sum_{mn} C^*_{mn} (S^{1/2})_{mn;k\ell}. \tag{9}$$

Once the orthogonalized CI expansion coefficients $\tilde{\mathbf{C}}$ are obtained, one may proceed normally with the standard Schmidt decomposition expressed in orthonormal basis sets, i.e., from Eq. (5) onwards. Although this method works well, it is impractical when using huge CI expansions (in the present work for H_2^+ with up to 140 000 basis components). To compute the matrix $\mathbf{S}^{1/2}$ a previous diagonalization of the full overlap matrix $\mathbf{S}$ and its whole eigenvalue spectrum is required, and this represents a bottleneck in the present implementation of the Löwdin orthogonalization.

2. *General method for the nonorthogonal Schmidt decomposition*

Any Hermitian operator $\hat{O}$ can be represented in terms of orthogonal $\{|\tilde{\phi}_i, \tilde{\chi}_j\rangle\}$ and nonorthogonal basis sets $\{|\phi_i, \chi_j\rangle\}$, in the form

$$\hat{O} = \sum_{ij,k\ell} |\tilde{\phi}_i \tilde{\chi}_j\rangle \tilde{O}_{ij;k\ell} \langle\tilde{\phi}_k \tilde{\chi}_\ell| = \sum_{ij,k\ell} |\phi_i \chi_j\rangle O_{ij;k\ell} \langle\phi_k \chi_\ell|, \tag{10}$$

where for the orthogonal case $\tilde{O}_{ij;k\ell}$ corresponds to the matrix elements $\langle\tilde{\phi}_i \tilde{\chi}_j|\hat{O}|\tilde{\phi}_k \tilde{\chi}_\ell\rangle$. However, in the nonorthogonal case, since the completeness condition is expressed using the overlap matrix $\mathbf{S}$ as $\hat{1} = \sum_{ij,k\ell} |\phi_i \chi_j\rangle S^{-1}_{ij;k\ell} \langle\phi_k \chi_\ell|$, the object $O_{ij;k\ell}$ in (10) corresponds to an array built from the matrix elements as follows:

$$O_{ij;k\ell} = \sum_{k'\ell'} \sum_{i'j'} S^{-1}_{ij;k'\ell'} \langle\phi_{k'} \chi_{\ell'}|\hat{O}|\phi_{i'} \chi_{j'}\rangle S^{-1}_{i'j';k\ell}. \tag{11}$$

The trace of the operator $\hat{O}$ can be computed with any dummy orthonormal complete basis set $\{|\tilde{\psi}_m \tilde{\varphi}_n\rangle\}$, such that $\mathrm{Tr}[\hat{O}] = \sum_{mn} \langle\tilde{\psi}_m \tilde{\varphi}_n|\hat{O}|\tilde{\psi}_m \tilde{\varphi}_n\rangle$. By inserting $\hat{O}$ given by Eq. (10) one obtains

$$\mathrm{Tr}[\hat{O}] = \sum_{ij,k\ell} \tilde{O}_{ij;k\ell} \langle\tilde{\phi}_k \tilde{\chi}_\ell|\tilde{\phi}_i \tilde{\chi}_j\rangle = \sum_{ij,k\ell} O_{ij;k\ell} \langle\phi_k \chi_\ell|\phi_i \chi_j\rangle. \tag{12}$$

If $\hat{O}$ is the density operator corresponding to the pure state $|\Psi\rangle$ in Eq. (1) spanned in an orthonormal basis, then $\hat{\rho} = |\Psi\rangle\langle\Psi|$, $\tilde{\rho}_{ij;k\ell} = \tilde{C}_{ij} \tilde{C}^*_{k\ell}$, and $\mathrm{Tr}[\hat{\rho}] = \sum_{k\ell} |\tilde{C}_{k\ell}|^2 = (\mathbf{C}\mathbf{C}^\dagger)_{\mathrm{diag}} = 1$, the latter due to normalization. In the nonorthogonal case, the state expansion reads $|\Psi\rangle = \sum_{ij} C_{ij} |\phi_i \chi_j\rangle$, and, after some algebra, $\rho_{ij;k\ell} = C_{ij} C^*_{k\ell}$ with $\mathrm{Tr}[\hat{\rho}] = (\mathbf{C}\mathbf{S}\mathbf{C}^\dagger)_{\mathrm{diag}} = 1$. In conclusion, the decomposition of operators and their traces have formulas which are invariant regardless the use of orthogonal or nonorthogonal basis sets.

Now, to compute the reduced density operators $\hat{\rho}^u$ and $\hat{\rho}^v$, one may use dummy orthogonal complete basis sets, $\{|\tilde{\psi}_m\rangle\} \in \mathcal{H}_U$ and $\{|\tilde{\varphi}_n\rangle\} \in \mathcal{H}_V$, so that

$$\hat{\rho}^u = \mathrm{Tr}_v[\hat{\rho}] = \sum_n \langle\tilde{\varphi}_n| \sum_{ij;k\ell} C_{ij} C^*_{k\ell} |\phi_i \chi_j\rangle \langle\phi_k \chi_\ell|\tilde{\varphi}_n\rangle,$$

$$\hat{\rho}^v = \mathrm{Tr}_u[\hat{\rho}] = \sum_m \langle\tilde{\psi}_m| \sum_{ij;k\ell} C_{ij} C^*_{k\ell} |\phi_i \chi_j\rangle \langle\phi_k \chi_\ell|\tilde{\psi}_m\rangle.$$

After simple algebra, the matrix elements of the reduced density matrices are

$$\begin{aligned} \rho^u_{ik} &= \sum_{j\ell}^{N} C_{ij} S^v_{j\ell} C^*_{k\ell} = (\mathbf{C}\mathbf{S}^v\mathbf{C}^\dagger)_{ik}, \\ \rho^v_{j\ell} &= \sum_{ik}^{M} C^*_{k\ell} S^u_{ki} C_{ij} = (\mathbf{C}^\dagger\mathbf{S}^u\mathbf{C})_{j\ell}, \end{aligned} \tag{13}$$

expressions indicating that the computation of the reduced density matrices only requires simple multiplications involving the CI expansion coefficients matrix *and the reduced overlap matrices* (simplifying by far the computational cost). Once the reduced density matrices are calculated, one proceeds by solving the generalized eigenvalue problems

$$\begin{aligned} \boldsymbol{\rho}^u \mathbf{S}^u \mathbf{c}^u &= \Lambda \mathbf{c}^u, \quad \text{with } \mathbf{c}^{u\dagger} \mathbf{S}^u \mathbf{c}^u = \mathbf{1}, \\ \boldsymbol{\rho}^v \mathbf{S}^v \mathbf{c}^v &= \Lambda \mathbf{c}^v, \quad \text{with } \mathbf{c}^{v\dagger} \mathbf{S}^v \mathbf{c}^v = \mathbf{1}, \end{aligned} \tag{14}$$

from which the two sets of orthonormal Schmidt bases (that share the same eigenvalues λ) can be built as

$$|u_i\rangle = \sum_{m=1}^{M} c^u_{im} |\phi_m\rangle, \quad |v_j\rangle = \sum_{n=1}^{N} c^v_{jn} |\chi_n\rangle. \tag{15}$$

3. *Entanglement measures*

Once the eigenvalues of the reduced density matrices $\{\lambda\}$ are obtained by any means, they serve to quantify the entanglement content of the state by using the von Neumann S_{vN} and linear S_L entropies, defined as

$$S_{vN}[\hat{\rho}] = -\mathrm{Tr}[\hat{\rho} \log_2 \hat{\rho}], \quad S_L[\hat{\rho}] = 1 - \mathrm{Tr}[\hat{\rho}^2], \tag{16}$$

where the expressions apply to the reduced density operators. The entanglement of the pure state $|\Psi\rangle$ precludes the idempotency of the density operators for the reduced subsystems, thus indicating mixedness with $\mathrm{Tr}[\hat{\rho}^2] < 1$. The linear entropy is no more that an approximation to the von Neumann entropy, by expanding the $\log_2$ term, so that entanglement is quantified directly from the purity $\mathrm{Tr}[\hat{\rho}^2]$. Within our algebraic method, these quantities can be readily calculated with the eigenspectrum of the reduced density matrices

$$S_{vN} = -\sum_{i=1}^{\min(M,N)} \lambda_i \log_2 \lambda_i, \quad S_L = 1 - \sum_{i=1}^{\min(M,N)} \lambda_i^2. \tag{17}$$

It is understood that pure states whose entropies approach zero are quasiseparable and slightly entangled and the larger the departure from zero the greater the entanglement. Then,

states with a leading Schmidt occupation number $\lambda_1 = 1$ are not entangled at all. When Schmidt occupations are evenly distributed among the different λ's one expects a maximum entanglement content.

III. RESULTS

A. Illustrative results on model systems

1. Coupled particles within a two-dimensional box

Our first model system consist of two particles with masses m_1 and m_2 confined within a 2D box of lengths L_1 and L_2, with a coupling represented by the Hamiltonian

$$\hat{H} = \frac{\hat{p}_1^2}{2m_1} + \frac{\hat{p}_2^2}{2m_2} + \kappa\left[\frac{1}{2}(x_1+x_2)^2 + \left(x_1^2 x_2 - x_1 x_2^2\right)\right] \quad (18)$$

with coordinates defined in the domains $x_1 \in [0, L_1]$ and $x_2 \in [0, L_2]$. The coupling is neither even nor odd against changes $x_1 \to x_2$ or $x_i \to -x_i$ $(i = 1,2)$, so that we avoid the presence of any geometrical symmetry in this system.

First, we have at our disposal complete orthonormal basis sets for the Hilbert subspaces $\mathcal{H}_{X_1}$ and $\mathcal{H}_{X_2}$, namely,

$$\phi_{n_1}(x_1) = \sqrt{\frac{2}{L_1}} \sin \frac{n_1 \pi x_1}{L_1}, \quad n_1 = 1, \dim[\mathcal{H}_{X_1}], \quad (19)$$

$$\phi_{n_2}(x_2) = \sqrt{\frac{2}{L_2}} \sin \frac{n_2 \pi x_2}{L_2}, \quad n_1 = 1, \dim[\mathcal{H}_{X_2}]. \quad (20)$$

Accordingly, the total CI wave function can be variationally expanded as [after Eq. (1)]

$$\Psi(x_1, x_2) = \sum_{n_1}^{\dim[X_1]} \sum_{n_2}^{\dim[X_2]} C_{n_1,n_2} \phi_{n_1}(x_1) \otimes \phi_{n_2}(x_2). \quad (21)$$

We choose a system with $m_1 = 4$, $m_2 = 1$, coupling strength $\kappa = 2$, and different length boxes $L_1 = 2$ and $L_2 = 4$. Dimensions for the basis sets in (19) and (20) are set to $\dim[\mathcal{H}_{X_1}] = 9$ and $\dim[\mathcal{H}_{X_2}] = 10$ (the basis is small to keep the simplicity of the illustration). After diagonalization of the total Hamiltonian matrix, 90 variational CI states are obtained, with energy eigenvalues for the lowest states quoted in Table I. In spite of the simplicity of the coupling potential, there is no exact solution for this system and particular quantum labels cannot be assigned to these eigenstates. Even the number of 1D nodal lines in the (x_1, x_2) plane hardly establish the energy ordering. As illustration, we plot the wave functions corresponding to the fourth and ninth eigenstates in Fig. 1 (that correspond to those with the highest entanglement content in Table I).

We choose to analyze the ninth lowest variational state (lower panel in Fig. 1). The 3D plots of wave functions for this and any other state obtained using (i) the full CI wave function in Eq. (21) with 90 terms and (ii) the Schmidt reconstruction using Eq. (3) with 9 terms are indistinguishable. The first Schmidt nonzero occupation numbers for this state (they must be nine) are $\lambda_1 = 0.64696$, $\lambda_2 = 0.31986$, $\lambda_3 = 0.024567$, $\lambda_4 = 0.0083872$, $\lambda_5 = 0.00021985$ (with the rest smaller by at least 2 orders of magnitude). The reduced Schmidt bases for the half spaces X_1 (the five most contributing) and X_2 (also five) are plotted in Fig. 2. It is worth noting that the Schmidt bases do not satisfy any particular property associated with eigenstates

TABLE I. Energy values and entanglement measures for the lowest ten eigenstates of two coupled particles within a 2D quantum box subject to the coupling potential quoted in Eq. (18). The energy eigenvalues are obtained using our variational CI method with both sine-type orthonormal (CI ort) and nonorthogonal (CI non-ort) B-polynomial basis sets. The von Neumann and linear entropies included in the table are those obtained using the CI nonorthogonal method.

	Energy (a.u.)		Entropies	
State	CI ort	CI nonort	S_{vN}	S_L
1	3.76176	3.76175	0.01537	0.00272
2	5.31181	5.31179	0.39113	0.13383
3	6.09695	6.09690	0.63680	0.24343
4	6.28873	6.28867	1.09801	0.48616
5	7.52299	7.52290	0.85700	0.34975
6	8.01306	8.01292	0.75063	0.27259
7	8.46759	8.46758	0.29608	0.08900
8	8.89911	8.89904	1.05092	0.47165
9	9.77130	9.77117	1.12442	0.47846
10	10.2020	10.2018	1.07954	0.39474

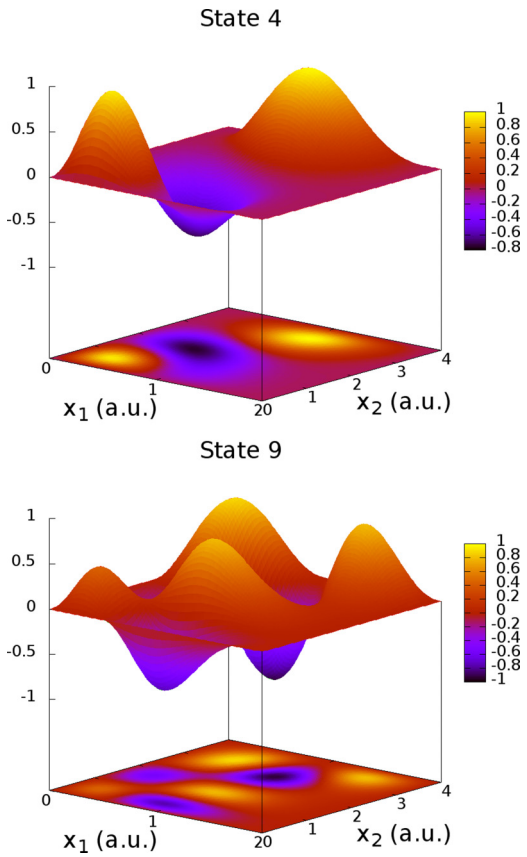

FIG. 1. Plot of the wave functions corresponding to the 4th and 9th eigenstates of two coupled particles within a 2D box with dimensions $L_1 = 2$ and $L_2 = 4$ a.u. for a Hamiltonian given by Eq. (18) and built as Schmidt decompositions using nonorthogonal B-polynomial basis sets (see text).

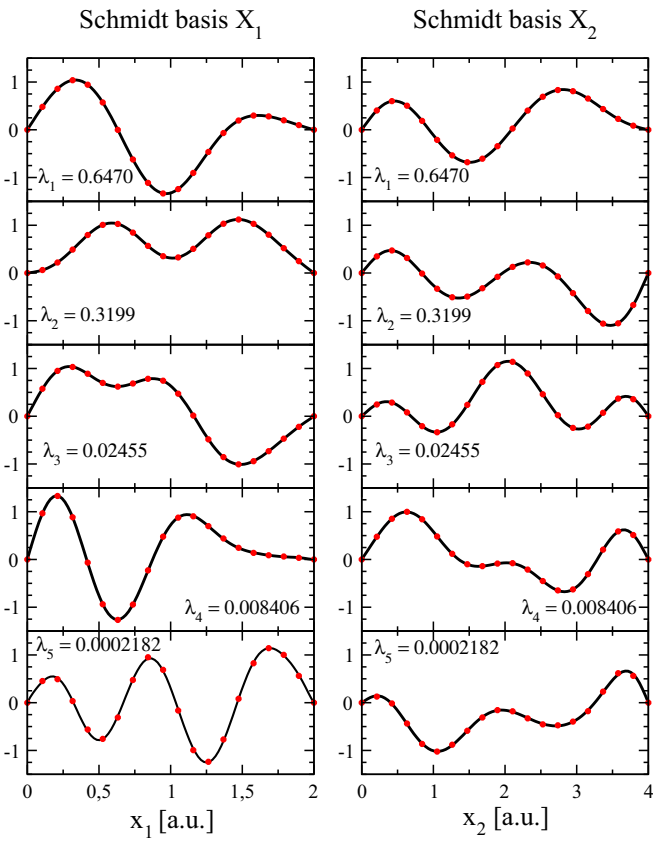

FIG. 2. Schmidt (orthogonal) basis as eigenvectors of the reduced density matrices, for two coupled particles confined in a 2D box with lengths $L_1 = 2$ a.u. and $L_2 = 4$ a.u. with coupling potential given in Eq. (18). Left panel: The first five Schmidt basis for half space X_1 using an orthonormal basis (solid line) and nonorthogonal B-polynomial basis (red circles), with their corresponding occupation number λ_i. Right panel: The same as in the left panel but for the first five Schmidt bases for half space X_2.

of one-dimensional Sturm-Liouville differential equations, like those related to the oscillation theorem and nondegeneracy [16]. The reduced density operators are Hermitian so that the Schmidt bases must be orthonormal, but orthogonality is not guaranteed by increasing numbers of nodes with the usual interpolating character. Also, in particular cases with high symmetry we found quasidegeneracies in the Schmidt eigenvalues. In the present case, the first Schmidt basis in half space X_1 (see Fig. 2) has two nodes, the second has no nodes at all, and the third basis has one node. Curiously, the Schmidt bases in half space X_2 seem to be the exception to the rule, with 2, 3, and 4 nodes for the first three functions, respectively, and interpolating to each other. But the rule is that no oscillation theorem generally applies.

We now select a suitable and simple nonorthogonal basis set, consisting of $n-1$ B-polynomials [17] defined within a box in the interval $[a,b]$ as follows (removing the first $k=0$ and the last $k=n$ elements to satisfy the boundary conditions of the quantum box):

$$B_{k,n}(x) = \binom{n}{k} \frac{(x-a)^k (b-x)^{n-k}}{(b-a)^n}, \quad 1 \leqslant k \leqslant n-1. \quad (22)$$

Matrix elements for the 1D problem in this basis are analytical and easy to obtain. The overlap matrix has elements

$$S_{ij} = \frac{n!^2 (i+j)!(2n-i-j)!}{i!j!(n-i)!(n-j)!(2n+1)!} L, \quad L = b-a, \quad (23)$$

and the kinetic energy matrix elements are

$$T_{ij} = -\frac{1}{2L} \frac{n!^2}{i!j!(n-i)!(n-j)!} \frac{(2n-i-j-2)!(i+j-2)!}{(2n-3)!} \times \frac{(i^2+j^2)n - (i+j)n + 2ij(1-n)}{2(2n-1}. \quad (24)$$

The matrix elements for the potential can be calculated with

$$(x^p)_{ij} = \frac{n!^2 (i+j+p)!(2n-i-j)!}{i!j!(n-i)!((n-j)!(2n+p+1)!} L^{p+1}. \quad (25)$$

B-polynomial basis sets have intrinsic disadvantages, namely, the calculation of large factorial numbers and that these bases rapidly display linear dependencies. Since our intention here is to provide a simple illustration with a small nonorthogonal basis set, B-polynomials fulfill well our requirements.

The variational wave function for the 2D problem can be expanded directly in terms of this basis set, i.e., $\Psi(x_1,x_2) = \sum_{i,j=1}^{m-1,n-1} C_{i,j} B_{m,i}(x_1) \otimes B_{n.j}(x_2)$, with $x_1 \in [0,L_1]$ and $x_2 \in [0,L_2]$. The full 2D overlap matrix is a Kronecker tensor product of 1D overlap matrices, $S_{ij,k\ell} = S^{x_1}_{i,k} \otimes S^{x_2}_{j,\ell}$, and the full 2D Hamiltonian is built similarly, $H_{ij,k\ell} = H^{x_1}_{i,k} \otimes S^{x_2}_{j,\ell} + S^{x_1}_{i,k} \otimes H^{x_2}_{j,\ell}$. Then the general eigenvalue problem $\boldsymbol{HC = ESC}$ is routinely solved. We have used the same parameters for the masses, box lengths, and coupling strength κ, and $\dim[X_1] = 11$ and $\dim[X_2] = 12$. Energy eigenvalues quoted in Table I compare very well with those obtained with the orthogonal case. The first five Schmidt nonzero occupation numbers for the ninth state (they must be eleven) are $\lambda_1 = 0.64696$, $\lambda_2 = 0.31986$, $\lambda_3 = 0.024553$, $\lambda_4 = 0.0084060$, $\lambda_5 = 0.00021821$, and they also compare very well with those obtained with the orthogonal basis, and the corresponding eigenfunctions (Schmidt bases) of the reduced density matrices are indistinguishable from those previously obtained (see Fig. 2). In addition, the results obtained using the Löwdin orthogonalization method applied to the B-polynomial basis (not included here) exactly coincide with those using our proposed nonorthogonal method, as expected.

The entanglement entropies for the lowest ten states are tabulated in Table I. We can appreciate that the behavior of entanglement is quite irregular. The ground state is barely entangled (which is a general rule due to a single dominant configuration) but entanglement does not always increase monotonically with the excitation energy. The present systems under study in this work contain distinguishable particles (or motions) and spin is not considered. This means that wave functions do not require any antisymmetrization procedure. Otherwise, the behavior could be quite different. For instance, in our previous study of entanglement in the He atom [18], the antisymmetry of the total wave function (with spin and spatial parts) along with the strong Coulomb coupling $1/r_{12}$ brings effects that make entanglement decrease monotonically against excitation within each mode given by a particular spectroscopic symmetry $^{2S+1}L^{\pi}$. If entanglement measures for all

modes in He (namely, $^3S^e$, $^{1,3}P^o$, and $^{1,3}D^e$) are put altogether, the behavior could be also quite irregular. Our conjecture is that entanglement always increases monotonically for interacting but distinguishable particles within a particular mode (also with an increasing number of nodes), provided one can identify exact or approximate modes. In the present illustrative case the system is simple but the coupling potential is complex enough to prevent a clear identification of modes. The entanglement content thus depends upon how complex is the topology of a given pure state regardless its excitation energy. In conclusion, for coupled but distinguishable particles, a higher entanglement is not univocally related to a higher excitation. To put these results in perspective and to clarify our conjecture we now analyze the entanglement content for a coupled but exactly solvable 2D system with a series of modes.

2. Coupled oscillators in a two-dimensional space

Now let us assume a model Hamiltonian in 2D with an exact solution and with an inversion symmetry, that consists of two coupled harmonic oscillators with masses m_1 and m_2 and corresponding Hooke constants $k_1 = m_1\omega_1^2$, $k_2 = m_2\omega_2^2$, and κ, the latter for the coupling term, as follows:

$$\hat{H} = \frac{\hat{p}_1^2}{2m_1} + \frac{\hat{p}_2^2}{2m_2} + \frac{1}{2}m_1\omega_1^2\hat{x}_1^2 + \frac{1}{2}m_2\omega_2^2\hat{x}_2^2 + \frac{1}{2}\kappa(\hat{x}_1 - \hat{x}_2)^2, \tag{26}$$

with the coordinates $x_1,x_2 \in (-\infty,+\infty)$. This choice now implies that the potential is invariant against an inversion symmetry operation ($x_i \to -x_i$, $i = 1$ and 2) and consequently the eigenstates must be gerade or ungerade with respect to inversion. This must have consequences in the building process of the Schmidt basis in $\mathcal{H}_{X_1}$ and $\mathcal{H}_{X_2}$: the reduced density matrices must be in block diagonal form, with two separated blocks (even and odd), and their eigenvectors must be even or odd against ($x_1 \to -x_1$) or ($x_2 \to -x_2$) operations.

Now, introducing the scaling $\hat{X}_1 = (m_1/m_2)^{1/4}\hat{x}_1$ and $\hat{X}_2 = (m_2/m_1)^{1/4}\hat{x}_2$ for the coordinates and $\hat{\mathcal{P}}_1 = (m_2/m_1)^{1/4}\hat{p}_1$ and $\hat{\mathcal{P}}_2 = (m_1/m_2)^{1/4}\hat{p}_2$ for the momenta, the Hamiltonian reads

$$\begin{aligned}\hat{H} = {} & \frac{\hat{\mathcal{P}}_1^2}{2\mu} + \frac{\hat{\mathcal{P}}_2^2}{2\mu} + \frac{1}{2}\mu\omega_1^2\hat{X}_1^2 + \frac{1}{2}\mu\omega_2^2\hat{X}_2^2 \\ & + \frac{1}{2}\kappa[(m_2/m_1)^{1/4}\hat{x}_1 - (m_1/m_2)^{1/4}\hat{x}_2]^2,\end{aligned} \tag{27}$$

where $\mu = (m_1m_2)^{1/2}$. An orthogonal transformation (rotation matrix with angle given by $\theta = \frac{1}{2}\arctan[\frac{2\kappa/\mu}{\omega_2^2-\omega_1^2+\kappa(m_1-m_2)/\mu^2}]$ for coordinates and momenta can bring the Hamiltonian to its diagonal uncoupled form in terms of normal modes:

$$\hat{H} = \frac{\hat{p}_+^2}{2\mu} + \frac{\hat{p}_-^2}{2\mu} + \frac{1}{2}\mu\omega_+^2\hat{x}_+^2 + \frac{1}{2}\mu\omega_-^2\hat{x}_-^2, \tag{28}$$

where the frequency modes are given by

$$\begin{aligned}\omega_+ = {} & \Big\{\omega_1^2\cos^2\theta + \omega_2^2\sin^2\theta \\ & + \frac{\kappa}{\mu}[(m_1/m_2)^{1/4}\sin\theta - (m_2/m_1)^{1/4}\cos\theta]^2\Big\}^{1/2},\end{aligned}$$

$$\begin{aligned}\omega_- = {} & \Big\{\omega_1^2\sin^2\theta + \omega_2^2\cos^2\theta \\ & + \frac{\kappa}{\mu}[(m_1/m_2)^{1/4}\cos\theta + (m_2/m_1)^{1/4}\sin\theta]^2\Big\}^{1/2},\end{aligned} \tag{29}$$

that yields exact energies $E_{n_+,n_-} = \omega_+(n_+ + 1/2) + \omega_-(n_- + 1/2)$, and exact eigenstates in the coordinate system for normal modes as a direct product $\Psi_{n_+,n_-}(x_+,x_-) = \varphi_{n_+}(x_+) \otimes \varphi_{n_-}(x_-)$, where

$$\varphi_{n_\pm}(x_\pm) = \left(\frac{\alpha_\pm}{\sqrt{\pi}2^{n_\pm}n_\pm!}\right)^{1/2}(-1)^{n_\pm}e^{-\alpha_\pm^2x_\pm^2/2}H_{n_\pm}(\alpha_\pm x_\pm) \tag{30}$$

are the well-known solutions for the harmonic oscillator, with $\alpha_\pm = (\mu\omega_\pm)^{1/2}$ and the Hermite polynomials $H_n(x)$.

Here it is important to remark that the entanglement content of a bipartite system depends on the choice for the splitting of half spaces. If subspaces are taken to be those corresponding to normal modes x_+,x_- any pure state of the system is clearly separable and not entangled, but if subspaces are taken according to the original coordinates $\{x_1,x_2\}$ any eigenstate is coupled and entangled. This is quite subtle and it precludes associating an absolute entanglement value to a composite state: the entanglement depends on the chosen half spaces.

For this particular system, we now choose to solve our system of coupled oscillators in Hilbert half spaces $\mathcal{H}_{X_1}$ and $\mathcal{H}_{X_2}$ with an expansion in terms of an even tempered Gaussian basis set with the form $\varphi_{n_i}(x_i) = \mathcal{N}_{n_i,\alpha_{n_i}}x^{n_i}e^{-(\alpha_{n_i}x_i)^2}$ (for $i = 1,2$ and $0 \leqslant n_i \leqslant N_i^{\max}$), with the normalization factor $\mathcal{N}_{n_i,\alpha_{n_i}} = \sqrt{\frac{2^{n_i}}{(2n_i-1)!!}}(\frac{(2\alpha_{n_i}^2)^{2n_i+1}}{\pi})^{1/4}$ and a geometrical sequence for the exponents $\alpha_{n_i} = \alpha_{0,i}/\gamma^{n_i}$, with $\alpha_{0,i} = \frac{1}{\sqrt{2}}[m_i(k_i+\kappa)]^{1/4}$ and $\gamma = 1.2$ (chosen to avoid linear dependencies within the basis set). All required single-particle matrix elements (overlap, kinetic energy, and potential) can be calculated analytically with the integral

$$\begin{aligned}&\int_{-\infty}^{\infty} x_i^{n_i+n_i'+k}e^{-(\alpha_{n_i}^2+\alpha_{n_i'}^2)x_i^2}dx_i \\ &\quad = \frac{1}{2}[1+(-1)^{n_i+n_i'+k}]\frac{1}{\left(\alpha_{n_i}^2+\alpha_{n_i'}^2\right)^{(n_i+n_i'+k+1)/2}} \\ &\qquad \times \frac{(n_i+n_i'+k-1)!!\sqrt{\pi}}{2^{(n_i+n_i'+k)/2}}\end{aligned} \tag{31}$$

for $i = 1,2$ and the construction of the full 2D Hamiltonian and overlap matrices follows the same guidelines as described for B-polynomials.

Let us take for this model the values $m_1 = 1$, $m_2 = 3$, $k_1 = 2$, $k_2 = 5$, and $\kappa = 7$. In this case, the normal mode frequencies are $\omega_+ = 3.3544$ and $\omega_- = 1.3221$, from which exact energies are obtained. We make use of 15 Gaussian basis sets for $\mathcal{H}_{X_1}$ and 16 Gaussians for $\mathcal{H}_{X_2}$ to expand a variational CI wave function. CI energies with 240 two-particle configurations are tabulated in Table II. Energies compare reasonably well with the exact ones, although the size of the variational basis set is clearly insufficient for highly excited states. This is of secondary importance. The correspondence

TABLE II. Energy values and entanglement measures for the lowest eigenstates of two coupled harmonic oscillators in a 2D space. Energy values are obtained from our variational CI method and they are compared with energies (not the same energy ordering) of the exact eigenstates, whose quantum numbers correspond to excitations (n_+,n_-) of normal modes (see text).

	Energy (a.u.)		Modes	Entropies	
State	CI	Exact	(n_+,n_-)	S_{vN}	S_L
1	2.3391	2.3382	(0,0)	0.24502	0.074229
2	3.6680	3.6602	(0,1)	0.90648	0.41682
3	5.0247	4.9823	(0,2)	1.3023	0.55517
4	5.7020	5.6927	(1,0)	0.90282	0.41524
5	6.4559	6.3044	(0,3)	1.5985	0.63781
6	7.0971	7.0147	(1,1)	1.5554	0.62251
7	7.9961	7.6264	(0,4)	1.8260	0.68651
8	8.6461	8.3368	(1,2)	1.8432	0.69444
9	9.1623	9.0471	(2,0)	1.2751	0.53968
10	9.6580	8.9485	(0,5)	1.9574	0.70762
11	10.431	9.6588	(1,3)	2.0063	0.71562
12	10.798	10.369	(2,1)	1.8981	0.70265
13	11.457	10.271	(0,6)	2.0014	0.71102
14	12.458	10.981	(1,4)	2.0997	0.74527
15	12.864	11.691	(2,2)	2.0169	0.73178
16	13.035	12.402	(3,0)	1.4265	0.57336
17	13.413	11.593	(0,7)	2.0017	0.71221
18	14.695	12.302	(1,5)	2.2487	0.75317

between the CI wave functions and the exact ones is made not only by comparing the energies but mainly through their topology and nodal lines in the plane (x_1,x_2). In Fig. 3 we plot the wave functions for the sixth (gerade) and eighth (ungerade) states, as reconstructed using the Schmidt decomposition with 15 terms in the expansion. The two plots are identical to those obtained with the full variational CI expansion and also with the Löwdin orthogonalization procedure, and they only present tiny differences when compared to the exact ones $\Psi_{1,1}(x_1,x_2)$ and $\Psi_{1,2}(x_1,x_2)$, respectively.

At this point, a remark is mandatory. The computational solution of any eigensystem brings an arbitrary phase for each eigenstate. The total CI wave functions and also the Schmidt bases for $\mathcal{H}_{X_1}$ and $\mathcal{H}_{X_2}$ are obtained from different separate diagonalizations. This is not a particular problem for the CI state, because it consists of a global phase, easily amended. The Schmidt reconstruction is made with a sum of direct products of Schmidt bases. One could fix the phase for each individual Schmidt function, for instance, to be defined as a positive function on the far left of a given coordinate axis. But there is no clue about how to determine the correct phase of each term within the sum in the Schmidt decomposition. The only procedure we devise is to project each Schmidt configuration with the total CI wave function; i.e., the term $\langle u_i v_i|\Psi\rangle/\sqrt{\lambda_i}$ must yield $+1$ or -1 and, therefore, the choice of a phase for each individual Schmidt basis is indeed irrelevant. Then, in practice, the Schmidt decomposition must be replaced by

$$|\Psi\rangle = \sum_{i=1}^{\min(M,N)} \mathrm{sgn}(i)\sqrt{\lambda_i}|u_i,v_i\rangle. \qquad (32)$$

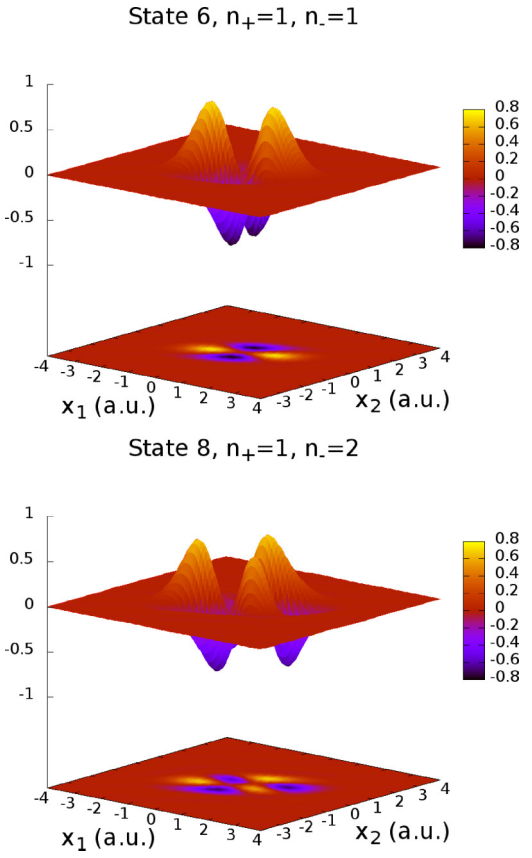

FIG. 3. Plot of the wave functions corresponding to the 6th (gerade) and 8th (ungerade) eigenstates of two coupled oscillators in 2D built as a Schmidt decomposition. These plots are identical to those obtained from the variational CI wave function and almost indistinguishable from the exact wave functions with excitations in normal modes $(n_+,n_-) = (1,1)$ and $(1,2)$, respectively.

Schmidt bases for both half spaces $\mathcal{H}_{X_1}$ and $\mathcal{H}_{X_2}$ corresponding to the sixth lowest eigenstate (top panel in Fig. 3) are included in Fig. 4 with the corresponding Schmidt occupation numbers λ's. The Gaussian basis set contains even and odd powers for x_1^n and x_2^n, and the reduced matrices for the subspaces have two separated blocks corresponding to even and odd eigenstates. To reproduce a gerade state (sixth state in Fig. 3) with Eq. (32), two Schmidt bases with the same λ and parity are combined (see Fig. 4). For any ungerade state (see bottom panel in Fig. 3) two Schmidt basis with the same λ but opposite parity must be combined. Additionally, the results obtained through a Löwdin orthogonalization method are identical to those obtained with our nonorthogonal method (see also results in Fig. 4).

The utility of this toy model is that we have an exact solution at our disposal in terms of normal modes (n_+,n_-) with coordinates (x_+,x_-). This help us to approximately classify our CI eigenstates solved with coordinates (x_1,x_2). From the occupation numbers λ_i obtained from the reduced density matrices in $\mathcal{H}_{X_1}$ and $\mathcal{H}_{X_2}$ we calculate the von Neumann and linear entropies and the values are tabulated in Table II and also plotted in Fig. 5, where we have associated with each point computed in $(\mathcal{H}_{X_1},\mathcal{H}_{X_2})$ the corresponding labels (n_+,n_-) for normal modes in $(\mathcal{H}_{X_+},\mathcal{H}_{X_-})$. The general behavior of

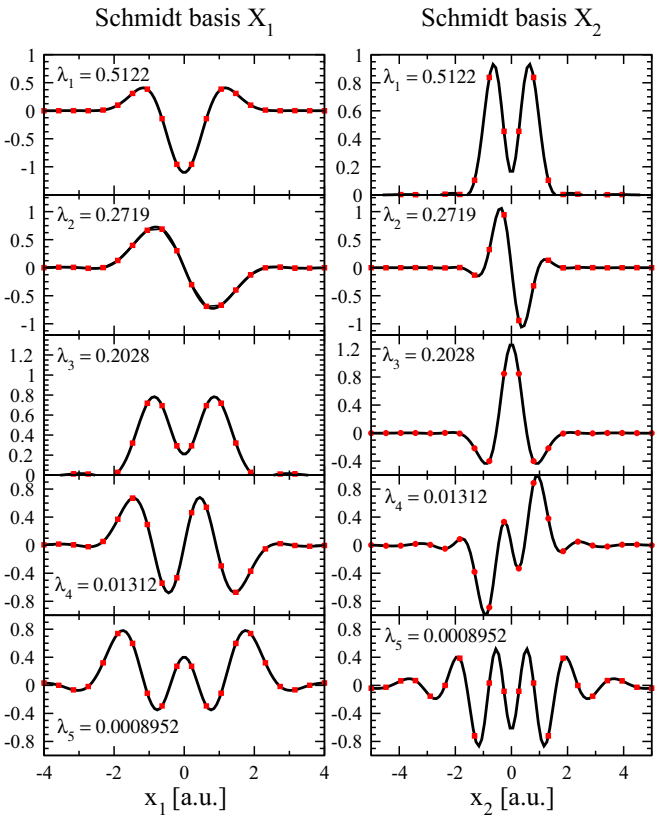

FIG. 4. Schmidt (orthogonal) basis as eigenvectors of the reduced density matrices extracted from the sixth eigenstate (gerade) of two coupled harmonic oscillators with Hamiltonian given in Eq. (26). Left panel: The first five Schmidt bases for half space X_1 with their corresponding occupation number λ_i using nonorthogonal Gaussian bases (solid line) and orthogonalized Gaussians *a la* Löwdin (red squares). Right panel: The same as in the left panel but for the first five Schmidt bases for half space X_2.

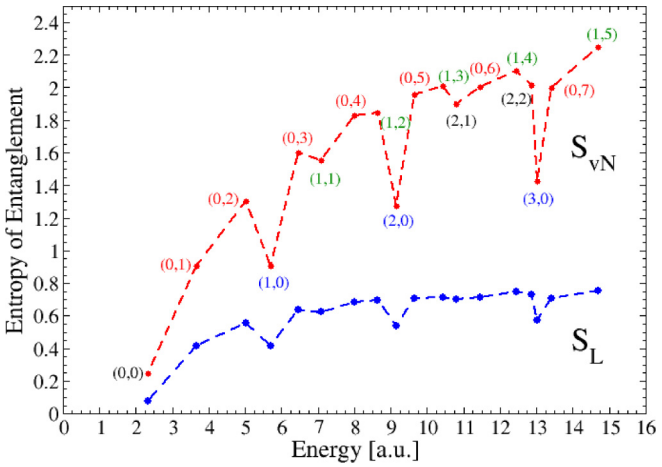

FIG. 5. Von Neumann (red circles) and linear entropies (blue squares) for the lowest eighteen eigenstates of two coupled harmonic oscillators in 2D with parameters $m_1 = 1$, $m_2 = 3$, $k_1 = 2$, $k_2 = 5$, and $\kappa = 7$ using a variational CI expansion in terms of (nonorthogonal) Gaussian basis sets. The entropies are calculated using Eq. (17) using the Schmidt occupation numbers $\{\lambda_i\}_{i=1}^{15}$. The labels (n_+,n_-) corresponding to excitations of normal modes for the exact eigenstates are used here to approximately identify the variational CI states (see text). The dashed lines are used to guide the eye and connect the consecutive values. It is observed that different excitation series $(0,n_-)$, $(n_+,0)$, $(1,n_-)$, $(n_+,1)$, etc., can be distinguished with notably different entanglement content.

entanglement seems to be increasing against excitation, again with irregularities. However, once the entanglement values are assigned to a given normal mode, the trend is much more clear. First, the entanglement content depends on the type of excitation manifold. For instance, the excitation series $(0,n_-)$ (higher entanglement) is clearly distinguished from the series $(n_+,0)$ (lower entanglement). Additional series can be guessed in Fig. 5 such as $(1,n_-)$ for $n_- \geqslant 1$ or $(n_+,1)$ for $n_+ \geqslant 1$. The arrangement of entanglement values in terms of excitation modes sheds light on our previous results for two coupled particles confined in a box. A general rule can now be established for quantum systems of distinguishable particles: the entanglement content increases monotonically against excitation *within* each excitation mode.

The entanglement value seems to saturate for high excitation energies, although in principle there is no rule for such an entanglement upper bound in this case (for the opposite behavior with fermions, that show a limiting value, the reader is referred to Ref. [18]). In principle, this monotonic increase within an excitation mode is due to the increasing participation of Schmidt bases with smaller occupation numbers, since the latter bases are responsible for reproducing the increasing number of oscillations and nodes in the reconstruction of the total wave function. For example, for the fifth state, labeled as (0,3), the first relevant Schmidt occupation numbers are $\lambda_1 = 0.4275$, $\lambda_2 = 0.3924$, $\lambda_3 = 0.1579$, $\lambda_4 = 0.0218$, and $\lambda_5 = 0.002424$, that yields $S_{vN} = 1.5989$. For the thirteenth state, within the same excitation mode, (0,6), the first relevant occupation numbers are $\lambda_1 = 0.3807$, $\lambda_2 = 0.3292$, $\lambda_3 = 0.1634$, $\lambda_4 = 0.0899$, $\lambda_5 = 0.02906$, and $\lambda_6 = 0.007573$ that gives $S_{vN} = 2.0014$. In the second case, the oscillations present in the total wave function due to six nodal lines are better reproduced by incorporating Schmidt basis with a higher oscillatory structure, thus reducing the occupation of the first Schmidt basis in comparison to those of the state (0,3), whose more simple nodal structure can be reproduced fairly well by using only the first three Schmidt basis pairs.

In addition, if we compare the entanglement of the pairs $(0,n_-)$ and $(n_+,0)$ for $n_+ = n_-$, i.e., (0,1)-(1,0) (2nd and 5th states, respectively), (0,2)-(2,0) (3rd and 9th), and (0,3)-(3,0) (5th and 16th), it is to note that although excitations with the smaller frequency mode ω_- have more entanglement content than excitations with larger frequency mode ω_+, the difference is relatively small, thus indicating that the number of nodal surfaces is closely linked to the entanglement. Finally, linear entropies S_L in Table II and Fig. 5 run parallel to the von Neumann entropy and it does not provide more information since it is a linearization of the von Neumann entropy.

B. Electronic-nuclear entanglement in hydrogen molecular ion

In this section we make use of the Schmidt-decomposition theorem using the nonorthogonal basis set formalism, to evaluate the entanglement between the electronic and nuclear

motions in the most simple one-electron molecule, H_2^+, for the $^2\Sigma_g^+$ symmetry. In addition, Schmidt natural orbitals for the electronic and nuclear motions are computed from the Schmidt decomposition of a non-BO total wave function.

To keep the problem more simple, we do not consider the nuclear rotation. Thus, the bipartite system in the one-electron molecular problem with three particles (nuclei with charges Z_a and Z_b and one electron) consist of separating the vibration and the electronic motion in two half spaces $\mathcal{H}_R$ and $\mathcal{H}_\mathbf{r}$. Then we solve the total Schrödinger equation $(\mathcal{H}-E)\Psi_n(\mathbf{r},R)=0$, with the nonrelativistic Hamiltonian

$$\hat{\mathcal{H}} = -\frac{1}{2\mu_{\rm nu}}\frac{d^2}{dR^2} + \frac{Z_a Z_b}{R} - \frac{1}{2\mu_{\rm el}}\nabla_r^2 - \frac{Z_a}{r_a} - \frac{Z_b}{r_b}, \quad (33)$$

where $\mu_{\rm nu}=m_p/2$ and $\mu_{\rm el}=m_p/(m_p+1)$ (m_p is the proton mass) indicate the reduced nuclear and electronic masses, respectively.

Our variational solution uses a one-center partial wave expansion for the electron with origin at the midpoint of the internuclear axis [19,20], and another expansion for the nuclear vibration. We use a basis set of B-splines for the relative motion of nuclei and the radial part of the electronic motion in the form [12]

$$\Psi_n(r,\theta,R) = \sum_{\alpha=1}^{N_{nu}}\sum_{i=1}^{N_{\rm el}}\sum_{\ell=0}^{\ell_{\rm max}} C^n_{\alpha i\ell} B_\alpha(R)\frac{B_i(r)}{r}\xi_\ell(\theta) \quad (34)$$

with the angular part of the electronic motion represented by

$$\xi_\ell(\theta) = \sqrt{\frac{2\ell+1}{2}}P_\ell(\cos\theta), \quad (35)$$

where $P_\ell(x)$ are the Legendre polynomials. Since we consider here the gerade symmetry for $^2\Sigma_g^+$ states, only even partial waves contribute in the sum over ℓ. We solve the eigenvalue problem $(\mathbf{H}-E\mathbf{S})\mathbf{C}=0$ where the matrix elements for the Hamiltonian,

$$H_{\alpha i\ell,\alpha' i'\ell'} = \iiint B_\alpha B_i \xi_\ell \hat{\mathcal{H}} B_{\alpha'} B_{i'} \xi_{\ell'} \sin\theta d\theta dR dr, \quad (36)$$

and for the overlap matrix,

$$S_{\alpha i\ell,\alpha' i'\ell'} = \delta_{\ell\ell'}\int B_\alpha B_{\alpha'} dR \int B_i B_{i'} dr = \delta_{\ell\ell'} S^{\rm nu}_{\alpha,\alpha'} S^{\rm el}_{i,i'}, \quad (37)$$

are efficiently computed when using B-splines [11]. From the full density matrix for the state Ψ_n, $\rho^n_{\alpha i\ell,\alpha' i'\ell'} = C^n_{\alpha i\ell} C^{n*}_{\alpha' i'\ell'}$, we readily obtain the reduced density matrices for the electron and nuclear motions, i.e.,

$$\rho^{n,\rm el}_{i\ell,i'\ell'} = \sum_\alpha \rho_{\alpha i\ell,\alpha i'\ell'}, \quad (38)$$

$$\rho^{n,\rm nu}_{\alpha,\alpha'} = \sum_{i\ell} \rho_{\alpha i\ell,\alpha' i\ell}, \quad (39)$$

and from them the subsequent Schmidt eigensystem

$$(\boldsymbol{\rho}^{n,\rm el} S^{\rm el} - \lambda^{n,\rm el})\mathtt{V}^{n,\rm el} = 0, \quad (40)$$

$$(\boldsymbol{\rho}^{n,\rm nu} S^{\rm nu} - \lambda^{n,\rm nu})\mathtt{V}^{n,\rm nu} = 0 \quad (41)$$

is solved, where $\lambda^{n,\rm el}=\lambda^{n,\rm nu}=\lambda^n$. The Schmidt natural orbitals are built from these eigenvectors $\mathtt{V}$ and the chosen nonorthogonal basis; for the nuclear motion

$$\chi^n_k(R) = \sum_\alpha V^{n,\rm nu}_{k,\alpha} B_\alpha(R), \quad (42)$$

and for the electronic motion

$$\varphi^n_k(r,\theta) = \sum_{i\ell} V^{n,\rm el}_{k,i\ell}\frac{B_i(r)}{r}\xi_\ell(\theta). \quad (43)$$

The total molecular wave function $\Psi_n(\mathbf{r},R)$ can be now expanded in terms of the Schmidt bases

$$\psi_n(r,\theta,R) = \sum_i^{N_{\rm max}} {\rm sgn}(i)\sqrt{\lambda^n_i}\varphi^n_i(r,\theta)\chi^n_i(R), \quad (44)$$

where $N_{\rm max}={\rm min}[N_{nu}, N_{\rm el}\times(\frac{\ell_{\rm max}}{2}+1)]$.

It is worth noting that the nuclear and electronic probability densities can be straightforwardly calculated by using only their corresponding Schmidt bases and occupations, i.e.,

$$\rho^{\rm nu}_n(R) = \int |\Psi_n(r,\theta,R)|^2 r^2 \sin\theta dr d\theta = \sum_k^{N_{\rm max}} \lambda^n_k |\chi^n_k(R)|^2 \quad (45)$$

and

$$\rho^{\rm el}_n(r,\theta) = \int |\Psi_n(r,\theta,R)|^2 dR = \sum_k^{N_{\rm max}} \lambda^n_k |\varphi^n_k(r,\theta)|^2. \quad (46)$$

To compute the total non-BO wave function using the ansatz (34) we employ a basis of 100 B-spline polynomials for the electron radial coordinate r and also 100 B-spline bases for the nuclear coordinate R, using a box with length 14 a.u. in both cases and the partial wave expansion contains 14 Legendre polynomials, from $\ell=0$ to $\ell_{\rm max}=26$, accounting only for even values of ℓ since we are here concerned with $^2\Sigma_g^+$ states. The proton/electron mass ratio used in this work is $m_p/m_e=1836.152673$.

Our non-BO energies are obtained after diagonalization of a $140\,000\times140\,000$ eigenproblem using multiprocessor PETSc [21] and SLEPc [22] libraries and it takes around 12 hours of computer time to calculate 130 eigenstates using 100 processors in the HLRN (Germany) supercomputing facility. The lowest seventeen eigenvalues that could be compared with the bound vibrational states supported by the BO $1s\sigma_g$ electronic state, up to the dissociation limit $H(1s)+H^+$ at $E=-0.5$ a.u., are included in Table III. Also, the eigenvalues that range from the 91st to the 100th, to be compared with the vibrational states of the BO $3d\sigma_g$ electronic state, are also quoted in Table III. Our goal was not to obtain benchmark energy results for the lowest roots (for example, our computed ground state energy is -0.5970726 a.u. to be compared with the highly accurate value -0.5971391 a.u. in [23]), but to accommodate a large spectrum of eigenvalues.

The nuclear probability density for all variational non-BO vibronic states below $E=-0.1$ a.u. (the rest above are not plotted) obtained after diagonalization are represented in Fig. 6. In spite of our huge expansion the representation has clear limitations for the dissociative states due to the chosen nuclear box of 14 a.u. Also, because of the box representation,

TABLE III. Non-BO energies (in a.u.) and linear S_L and von Neumann S_{vN} entropies for the lowest seventeen $^2\Sigma_g^+$ states, located below the first dissociation limit $H(1s) + H^+$ ($E = -0.5$ a.u.). These states compare well with the vibrational levels of the H_2^+ molecular ion bound by the $1s\sigma_g$ potential energy curve within the BO approximation; similarly for the ten lowest non-BO states (from the 91st to the 100th eigenstate) that could be associated with the vibrational states bound by the higher $3d\sigma_g$ potential energy curve.

n	Energy (a.u.)	S_L	S_{vN}
		$1s\sigma_g$	
1	−0.5970726	0.0104556	0.0479102
2	−0.5870808	0.0309338	0.1183180
3	−0.5776665	0.0508738	0.1781296
4	−0.5688101	0.0704016	0.2324166
5	−0.5604945	0.0896266	0.2832269
6	−0.5527066	0.1086473	0.3317358
7	−0.5454358	0.1274887	0.3785935
8	−0.5386708	0.1461490	0.4242275
9	−0.5324040	0.1647812	0.4693102
10	−0.5266354	0.1835216	0.5144123
11	−0.5213654	0.2021833	0.5594135
12	−0.5165920	0.2205226	0.6041233
13	−0.5123154	0.2385122	0.6488478
14	−0.5085394	0.2560744	0.6938581
15	−0.5052646	0.2728426	0.7389355
16	−0.5024833	0.2884677	0.7839340
17	−0.5001705	0.3032127	0.8297232
		$3d\sigma_g$	
91	−0.1736249	0.0188649	0.0790464
92	−0.1716710	0.0534788	0.1856425
93	−0.1697621	0.0844051	0.2689602
94	−0.1678974	0.1122812	0.3391536
95	−0.1660758	0.1375620	0.4002939
96	−0.1642963	0.1605975	0.4546355
97	−0.1625577	0.1816465	0.5035563
98	−0.1608575	0.2007819	0.5476373
99	−0.1591843	0.2177013	0.5863670
100	−0.1575013	0.2318837	0.6187359

the energy gap between $E \sim -0.25$ and $E \sim -0.175$ a.u. is an artifact, and only the lowest lying bound vibronic states associated with the $3d\sigma_g$ are well represented. Anyway it suffices for our purposes in this work. In Fig. 6 one can appreciate that oscillations of the bound vibronic states end up at the turning points of the BO curves $1s\sigma_g$ and $3d\sigma_g$ and that, as expected here, they satisfy the oscillation theorem. Consequently, since oscillations increase, the number of participating Schmidt bases increases as well. We can say indeed that non-BO vibronic states in H_2^+ enter into different *hidden* electronic modes (BO $1s\sigma_g$, $3d\sigma_g$, $2s\sigma_g$, etc.). The entanglement content for the vibronic ground state within the two lowest electronic modes is similarly small ($S_{vN} = 0.0479102$ for the first state and $S_{vN} = 0.0790464$ for the 91st state), and from them, the entanglement entropy increases monotonically with excitation within each mode, as shown in Table III. Also, entanglement increases twice faster in the $3d\sigma_g$ mode than in the $1s\sigma_g$ one, mostly due to the higher spatial confinement or compactness of the nuclear density in the $1s\sigma_g$ manifold, as illustrated in Fig. 7 [in this figure the

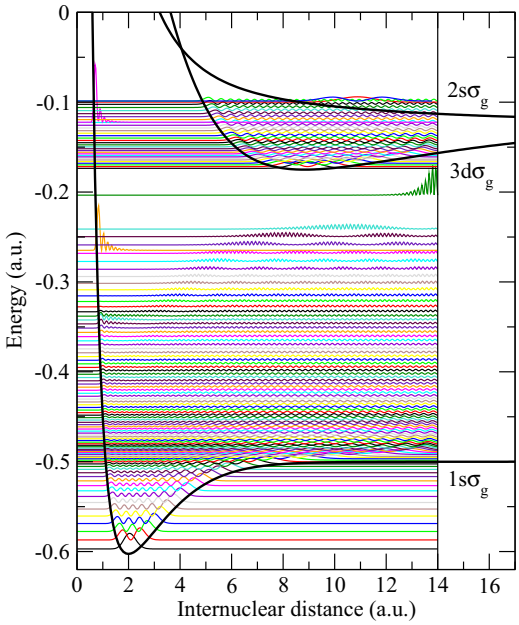

FIG. 6. Nuclear probability density for all non-BO vibronic states of H_2^+. Each nuclear probability density is calculated as $\rho_n^{\rm nu}(R') = \langle\Psi_n|\delta(R - R')|\Psi_n\rangle$ using Eq. (45) and it is shifted to its corresponding variational energy in the figure. The exact BO potential energy curves for states $^2\Sigma_g^+$ $1s\sigma_g$, $2s\sigma_g$, and $3d\sigma_g$ are also included in the figure to guide the eye.

nuclear probability density is computed by the two alternative forms in Eq. (45), with excellent agreement].

To validate our calculations we have compared our results with those of Ref. [13] for HD^+. This reference only gives the first Schmidt occupation numbers (λ) obtained from the analysis of the ground state with non-BO energy $E = -0.597\,897\,9686$ a.u., i.e., $\lambda_1 = 0.99629$, $\lambda_2 = 3.68 \times 10^{-3}$, $\lambda_3 = 2.48 \times 10^{-5}$, $\lambda_4 = 2.42 \times 10^{-7}$, $\lambda_5 = 2.6 \times 10^{-9}$, $\lambda_6 = 3.1 \times 10^{-11}$, that results in an entanglement $S_{vN}^{nBO} = 0.0354840$. Also, in Ref. [13], the authors provide occupation

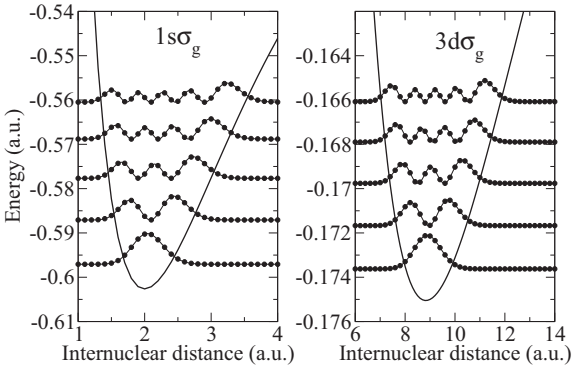

FIG. 7. The nuclear probability density for the non-BO vibronic states $n = 1$–5 associated with the BO potential $1s\sigma_g$ (left panel) and for the non-BO vibronic states $n = 91$–95, associated with the BO potential $3d\sigma_g$. Each probability density is referred to its corresponding vibronic energy quoted in Table III. Lines: Values calculated using the integral form in Eq. (45). Dots: Values calculated using the Schmidt sum in Eq. (45). The potential energy curves of BO states $1s\sigma_g$ and $2p\sigma_u$ are also included to guide the eye.

numbers for the natural orbitals computed within the BO approximation. Differences with the non-BO case are small and the resulting BO entanglement is $S_{vN}^{BO} = 0.0351404$. Importantly then, it is shown that the BO approximation already entails an electronic-nuclear entanglement and non-BO entanglement is quantified on top of this offset entanglement. Computations for HD^+ within our one-center method are even more involved than for H_2^+, due to the missing gerade/ungerade symmetry that makes necessary the use of both even and odd partial waves in the expansion (34). Also, we use a crude expansion in B-spline bases instead of in terms of optimized orbitals [13]. Then for the ground state we obtain the non-BO energy $E = -0.5978886$ a.u. and our first values for the Schmidt occupations are $\lambda_1 = 0.99515$, $\lambda_2 = 4.76 \times 10^{-3}, \lambda_3 = 7.89 \times 10^{-5}, \lambda_4 = 5.12 \times 10^{-6}$, for $S_{vN} = 0.04492$, which compares reasonably well. Eventually, this means that although our absolute values for the entanglement entropy in H_2^+ may have some systematic error, our relative differences are quantitatively sound.

Schmidt bases for H_2^+ can be computed for each non-BO vibronic state using the method outlined in Sec. II B for nonorthogonal bases. Its development is required since the Löwdin orthogonalization method is impractical for variational cases with such huge expansions. The latter method requires computing the matrices $\mathbf{S}^{\pm 1/2}$, which can be accomplished by first calculating the diagonal form of the overlap matrix $\mathbf{S}$. For instance, in our present case for H_2^+, the diagonalization of the matrix $\mathbf{S}$ with a size $140\,000 \times 140\,000$ and the manipulation of matrices $\mathbf{S}^{\pm 1/2}$ to compute the Schmidt basis is very demanding computationally. Instead, the present nonorthogonal method does not require the diagonalization of the overlap matrices and, furthermore, the computation of Schmidt bases becomes computationally cheaper through the involvement of overlap matrices of the reduced spaces in Eq. (13) with sizes 100×100 and 1400×1400. As an illustration we include in Fig. 8 the first series (and most contributing) of the electronic and nuclear Schmidt bases for the second ($n = 2$ in Table III) non-BO vibronic state. The participation of the first electronic-nuclear pair (top panel in Fig. 8) already dominates with $\lambda_1 = 0.984$ which indicates its small entanglement content. Also, the total wave function can be *almost* expressed as a direct product $\Psi_{n=2}(\mathbf{r},R) \sim \varphi_1^{n=2}(r,\theta) \times \chi_1^{n=2}(R)$. This form reminds us of the BO separation ansatz $\Phi_{v=1}^{1s\sigma_g}(\mathbf{r},R) = \varphi_{1s\sigma_g}(r,\theta;R) \times \chi_{v=1}^{1s\sigma_g}(R)$, but with a notable difference: the electronic Schmidt basis does not depend parametrically on the internuclear distance R. The vibrational Schmidt basis $\chi_1^{n=2}(R)$ (top panel in Fig. 8) is similar to the vibrational state $\chi_{v=1}^{1s\sigma_g}(R)$ and the electronic density of the chief Schmidt basis (without nodes) accumulates in the neighborhood of the two protons at a non-BO internuclear equilibrium distance. This is quite subtle; the BO electronic wave function $\varphi_{1s\sigma_g}(r,\theta;R)$ must be calculated at every single internuclear distance $R \in [0,+\infty)$ then just to be multiplied by the nuclear function $\chi_{v=1}^{1s\sigma_g}(R)$, which is only relevant in the interval $R \in [1,4]$ a.u.. The latter nuclear wave function acts as a weighting or damping factor for the electronic BO wave functions. The result is that whereas none of the BO functions at any $R \in [1,4]$ distance can be univocally compared to the unique Schmidt electronic basis $\varphi_1^{n=2}(r,\theta)$,

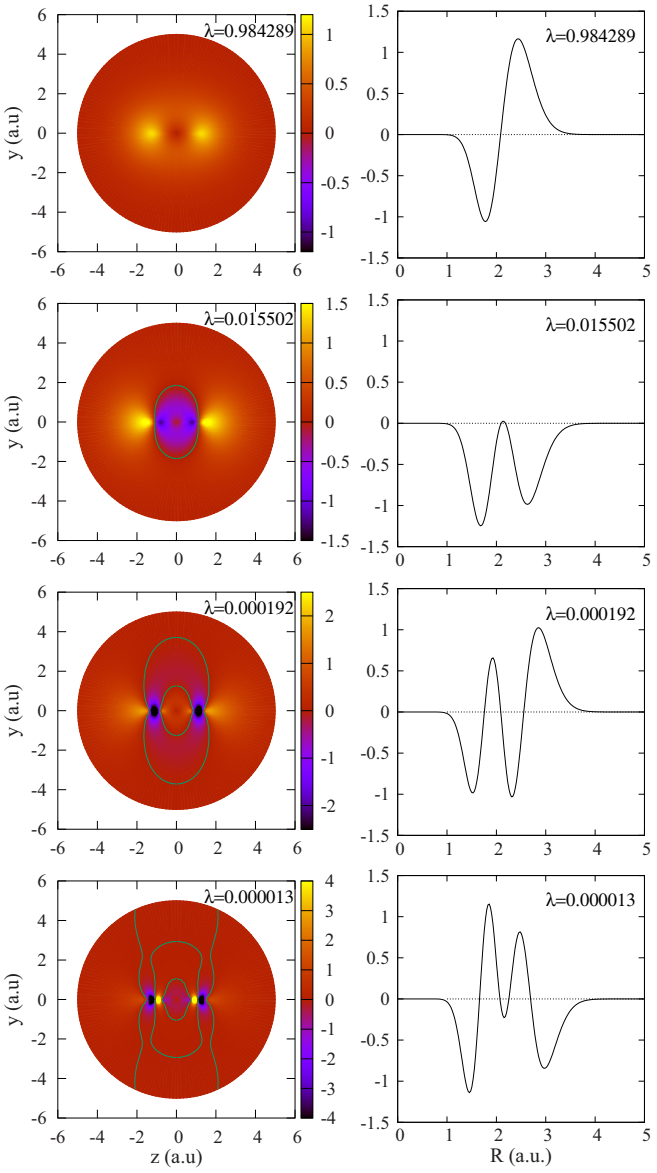

FIG. 8. Electronic (left panels) and nuclear (right panels) Schmidt natural orbitals corresponding to the non-BO vibronic state $n = 2$, associated with the second vibrational state of the BO potential energy curve $1s\sigma_g$. Nodal lines in the electronic Schmidt bases, where the density is zero, are indicated with green lines. In this case, they correspond to radial nodes.

both electronic-nuclear products yield a similar result for the total wave function of the second vibronic state, where the BO approximation works fine. In fact, the BO approximation works very well for all bound states in H_2^+ quoted in Table III. However, the entanglement entropy increases with excitation which means that, in principle, the entanglement content could be disconnected from the plausibility in the application of the BO approximation (see also [7]).

Similarly, we also include in Fig. 9 the corresponding Schmidt electronic and nuclear basis for the non-BO vibronic state $n = 93$ in Table III, that could be associated with the third vibrational state supported by the $3d\sigma_g$ state. The lowest Schmidt pair has $\lambda_1 = 0.9559$ and therefore it

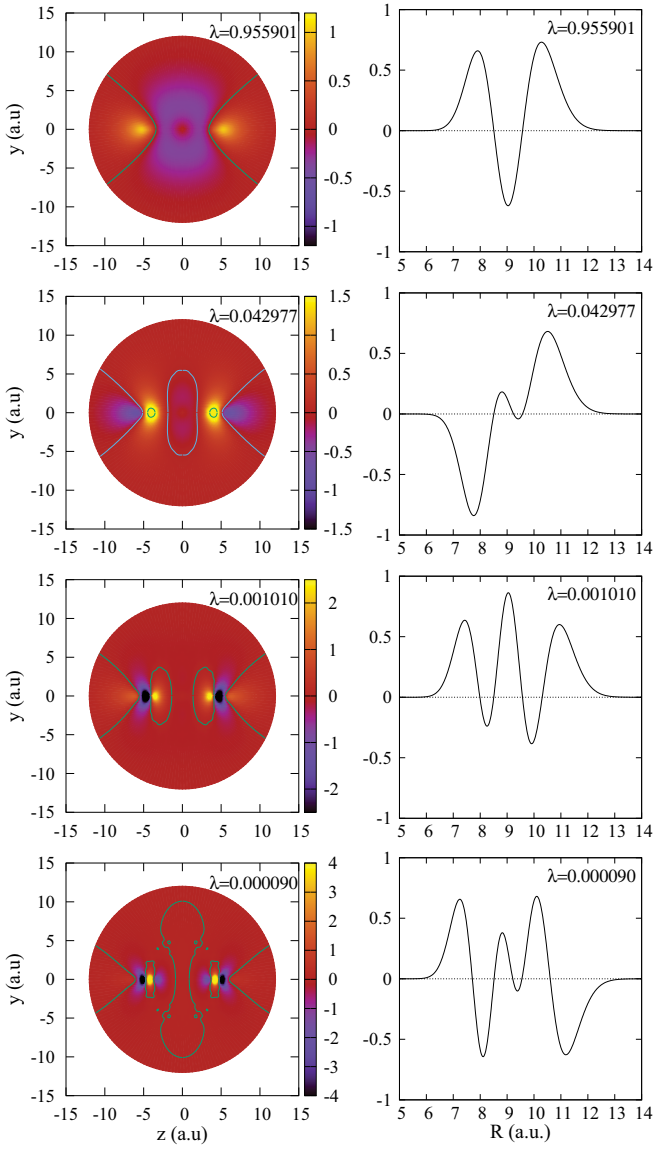

FIG. 9. Electronic (left panels) and nuclear (right panels) Schmidt natural orbitals corresponding to the non-BO vibronic state $n = 93$ in Table III, associated with the third vibrational state of the BO potential energy curve $3d\sigma_g$. Nodal lines in the electronic Schmidt bases, where the density is zero, are indicated with green lines. In this case, they correspond to both radial and angular nodes. The two angular nodes are invariant and present in all Schmidt bases, but the number of radial nodes increases.

almost reproduces the electronic and nuclear densities at the equilibrium distance of the $3d\sigma_g$ potential energy surface. The BO $3d\sigma_g$ state is known to have two angular nodes in the confocal elliptic coordinate $\eta = (r_1 - r_2)/2$, which is reproduced in all Schmidt electronic bases (left panels in Fig. 9). The dominant nuclear Schmidt basis (also in the top panel in Fig. 9) approximately reproduces the $\chi_{v=2}^{3d\sigma_g}(R)$ centered at $R = 9$ a.u. with two radial nodes.

To conclude, we include some analysis of the total non-BO wave functions of H_2^+. In principle, a non-BO solution cannot rely on the existence of potential energy curves but its scrutiny can be performed by computing some properties or

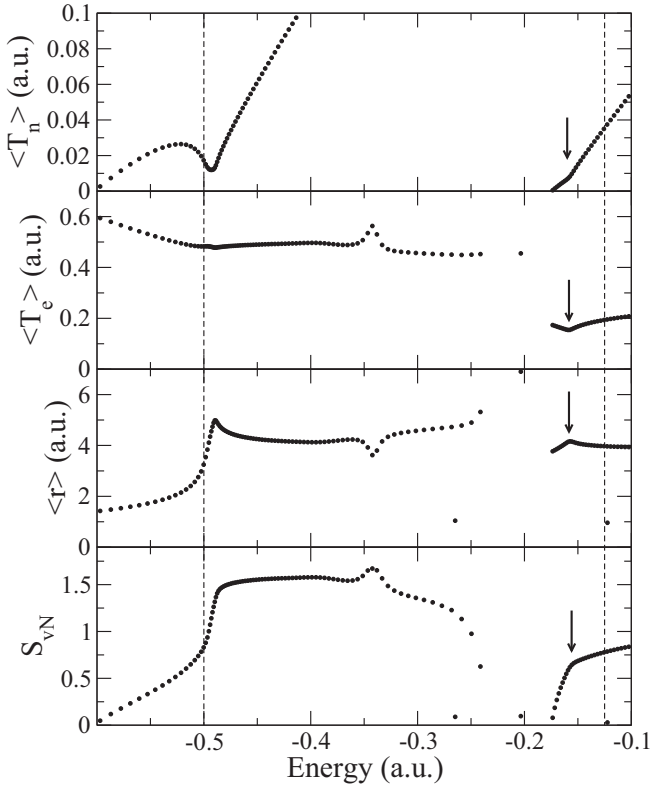

FIG. 10. From top to bottom: Expectation values of the kinetic energy operator of the nuclear T_n and electronic T_e motion, expectation value of the radial component of the position vector of the electron r, and von Neumann entropy S_{vN}. The dashed vertical lines at -0.5 and -0.125 a.u. indicate the dissociation thresholds of the $1s\sigma_g$ and $3d\sigma_g$ BO states of H_2^+. Vertical arrows indicate the upper limit until which the non-BO vibronic states are well represented within a nuclear box of 14 a.u.

expectation values. For instance, we compute the expectation values for the electron kinetic energy operator $\hat{T}_{\rm el} = -\frac{1}{2\mu_{\rm el}}\nabla^2_{\mathbf{r}}$ and the nuclear kinetic energy $\hat{T}_{nu} = -\frac{1}{2\mu_n}\frac{\partial^2}{\partial R^2}$ in Eq. (33). Also, the expectation value of the radial component r of the position vector $\mathbf{r}$ for the electron with origin located at the midpoint of the internuclear distance is evaluated. All these quantities are included in Fig. 10. For instance, the expectation value $\langle \hat{T}_{nu} \rangle$ shows a typical behavior for an anharmonic potential: the nuclear kinetic energy increases for the lowest states, which approximately follow the harmonic oscillator expectation value, reaches a maximum, and then its value decreases for vibrational Rydberg states. In the dissociation limit at $E = -0.5$ a.u. it connects with the nuclear continuum with zero kinetic energy. From this point, the kinetic energy of the fragments increases monotonically, as expected. At energy $E \sim -0.17$ a.u., $\langle \hat{T}_{nu} \rangle$ takes again a very small value, which indicates that the system reaches a new oscillatory motion within another electronic excitation mode (the BO $3d\sigma_g$). Unfortunately, due to limitations of our computation concerning a nuclear box of limited size, high-energy non-BO vibronic states associated with the BO $3d\sigma_g$ mode are not well represented around the second dissociation threshold at $E = -0.125$ a.u. (see Fig. 6) and, consequently,

the expectation value does not drop to zero as expected, but instead increases monotonically. The expectation value for the electronic kinetic operator decreases with excitation (to compensate the increasing value of the potential average) up to the well-known limit of $\langle T_e \rangle = 0.5$ a.u. for the hydrogen atom at $E = -0.5$ a.u. (according to the quantum virial theorem). Analogously to $\langle \hat{T}_{nu} \rangle$, the expectation values $\langle \hat{T}_e \rangle$ and $\langle r \rangle$ show clear discontinuities also at $E \sim -0.17$ a.u. indicating a transition to a new electronic mode of motion. The more striking issue corresponds to the entanglement measure, that also follows an analogous pattern. The entanglement increases monotonically within the lowest electronic mode $1s\sigma_g$ to reach the nuclear dissociation limit after which entanglement remains approximately constant (the constant value and the structures in the nuclear continuum are due to limitations in the correct representation of the density of states) to suddenly drop to a minimum value at $E \sim -0.17$ a.u. ($3d\sigma_g$ mode), from where again the entanglement increases monotonically within the second electronic mode of motion. In conclusion, this means that entanglement may also act as a witness to approximately elucidate to which electronic state or mode a full non-BO vibronic state belongs within blind non-BO molecular calculations.

IV. CONCLUSIONS AND PERSPECTIVES

A theoretical framework based on the Schmidt decomposition theorem suitable for nonorthogonal basis sets has been devised and applied to fully correlated non-BO eigenfunctions of the Hamiltonian representing a nonrotating H_2^+ molecule. This molecule can be established as a realistic prototype of a bipartite system to study entanglement between two distinguishable subsystems or motions, electronic motion plus nuclear vibration. This entanglement in the H_2^+ molecule has been quantified by calculating the von Neumann and linear entropies arising from the eigenvalues of the reduced density matrices. We find that the entanglement entropy associated with a non-BO wave function along with the expectation values for nuclear and electronic kinetic energies may serve as a criterion to associate the non-BO vibronic states with a given electronic BO potential energy curve or electronic excitation mode. It is also observed that, for the analyzed lowest non-BO vibronic states associated with $^2\Sigma_g^+$ $1s\sigma_g$ and $3d\sigma_g$ BO states, the dominant electronic and nuclear Schmidt bases display the main features of the BO electronic (at the equilibrium distance) and nuclear wave functions, respectively. This is more than reasonable since the BO approximation is fully justified in the cases reported in this work for H_2^+. This method will find more insightful applications in molecular systems that show avoided crossings or conical intersections between their BO curves, where the electronic-nuclear entanglement is expected to dominate. Nevertheless, it must be pointed out that the Schmidt decomposition theorem only applies to bipartite systems (such as two atomic electrons, two spins, electron plus vibration, or two coupled vibrational normal modes). That being so, the Schmidt separation in molecules can be established at most between global electronic (all electrons) and nuclear motions (including both rotation and vibration). At this point, an extension to the H_2 molecule (2 electrons + vibration) is feasible by considering spin-adapted two-electron configurations in terms of one-center B-spline expansions for the electronic motion, although this is very demanding computationally.

One must recognize that the use of the Schmidt decomposition theorem is very helpful to replace the total wave function in terms of a large CI expansion with a much shorter one, but in order to obtain the latter, the former is required for the reduction. It would be desirable to produce the bipartite Schmidt bases (even approximate) using a shortcut, yet unknown. Furthermore, the practical use of the Schmidt decomposition requires the knowledge of the relative signs in the superposition of Schmidt basis products, which is an important issue for highly entangled states where Schmidt occupations are evenly distributed. These phases, being put aside a trial and error procedure, are also obtained from the knowledge of the total CI wave function. Nevertheless, once the Schmidt bases are obtained for any particular vibronic state, and since they are formally complete, they can be used as universal basis sets to expand any molecular orbital or any vibrational state, with better convergence properties as is well known for natural orbitals in quantum chemistry [15].

There are different forms to write or expand the total molecular wave function $\Psi(\mathbf{r},\mathbf{R})$, namely, the Born-Huang ansatz $\Psi(\mathbf{r},\mathbf{R}) = \sum_i F_i^{nu}(\mathbf{R})\varphi_i^{\mathrm{el}}(\mathbf{r};\mathbf{R})$ in terms of eigenstates φ_i^{el} of the electronic Hamiltonian [24], the marginal and conditional exact factorization form $\Psi(\mathbf{r},\mathbf{R}) = f(\mathbf{R})P(\mathbf{r}|\mathbf{R})$ by Hunter [25,26] (that yields hard-to-solve coupled integro-differential equations) and the present Schmidt form $\Psi(\mathbf{r},\mathbf{R}) = \sum_i \sqrt{\lambda_i}\phi_i(\mathbf{r})\chi_i(\mathbf{R})$. The Born-Huang ansatz introduces the well-known nonadiabatic couplings among electronic states due to the kinetic operator, namely, matrix elements $\langle \varphi_i^{\mathrm{el}}|\nabla_R|\varphi_j^{\mathrm{el}}\rangle$ and $\langle \varphi_i^{\mathrm{el}}|\nabla_R^2|\varphi_j^{\mathrm{el}}\rangle$, since the electronic functions still depend parametrically on the nuclear geometry. At variance, these nonadiabatic couplings are missing when using the Schmidt form. However, other electrostatic couplings $\langle \phi_i|\hat{H}_{\mathrm{el}}\phi_j\rangle$ appear instead since the Schmidt electronic bases are not eigenfunctions of the electronic Hamiltonian. In this respect, they can be eventually proposed as *diabatic* basis to be used in molecular dynamics. However, its practical implementation must be taken with caution since both electronic and nuclear Schmidt bases obtained from a selected vibronic state (even with large expansions) span only a limited spatial region in the electronic and nuclear coordinates (for instance, some nuclear Schmidt bases span the interval $R \in [1,4]$ a.u. in Fig. 8 and others the interval $R \in [6,13]$ in Fig. 9). Ultimately, this implies that these wave functions could eventually be used in a piecewise form, by successively joining Schmidt bases that provide finite support in different intervals of the electronic and nuclear coordinates.

ACKNOWLEDGMENTS

J.L.S.-V. acknowledges financial support from Vicerrectoría de Investigación (Estrategia de Sostenibilidad) at Universidad de Antioquia and from Departamento Administrativo de Ciencia, Tecnología e Innovación (COLCIENCIAS), Colombia under Grant No. 111565842968. J.F.P.-T. acknowledges financial support from Universidad de Medellín through Internal Project No. 840 and Deutsche Forschungsgemeinschaft, under

Project No. PE-229/1-1 (Germany). We also thank North-German Supercomputing Alliance (HLRN) for the generous allocation of computing time. We thank Julio Arce for a critical reading of the manuscript.

[1] M. A. Nielsen and I. L. Chuang, *Quantum Computation and Quantum Information*, 1st ed. (Cambridge University Press, Cambridge, 2002).
[2] L. K. McKemmish, R. H. McKenzie, N. S. Hush, and J. R. Reimers, J. Chem. Phys. **135**, 244110 (2011).
[3] M. Vatasescu, Phys. Rev. A **88**, 063415 (2013).
[4] P. A. Bouvrie, A. P. Majtey, M. C. Tichy, J. S. Dehesa, and A. R. Plastino, Eur. Phys. J. D **68**, 346 (2014).
[5] L. K. McKemmish, R. H. McKenzie, N. S. Hush, and J. R. Reimers, Phys. Chem. Chem. Phys. **17**, 24666 (2015).
[6] M. Vatasescu, Phys. Rev. A **92**, 042323 (2015).
[7] A. F. Izmaylov and I. Franco, J. Chem. Theory Comput. **13**, 20 (2017).
[8] E. Schmidt, Math. Ann. **63**, 433 (1906).
[9] C. C. Gerry and P. L. Knight, *Introductory Quantum Optics*, 1st ed. (Cambridge University Press, New York, 2005).
[10] C. de Boor, *A Practical Guide to Splines* (Springer, New York, 1978).
[11] H. Bachau, E. Cormier, P. Decleva, J. E. Hansen, and F. Martín, Rep. Prog. Phys. **64**, 1815 (2001).
[12] J. F. Pérez-Torres, Phys. Rev. A **87**, 062512 (2013).
[13] D. J. Haxton, K. V. Lawler, and C. W. McCurdy, Phys. Rev. A **83**, 063416 (2011).
[14] P.-O. Löwdin, J. Chem. Phys. **18**, 365 (1950).
[15] A. Szabo and N. S. Ostlund, *Modern Quantum Chemistry*, 1st ed. (McGraw-Hill Pub. Co., New York, 1982).
[16] L. Landau and E. Lifshitz, *Quantum Mechanics: Non Relativistic Theory*, 1st ed. (Pergamon Press, Oxford, 1965).
[17] M. I. Bhatti and W. F. Perger, J. Phys. B: At., Mol. Opt. Phys. **39**, 553 (2006).
[18] J. P. Restrepo Cuartas and J. L. Sanz-Vicario, Phys. Rev. A **91**, 052301 (2015).
[19] M. Brosolo, P. Decleva, and A. Lisini, J. Phys. B: At., Mol. Opt. Phys. **25**, 3345 (1992).
[20] F. Martín, J. Phys. B: At., Mol. Opt. Phys. **32**, R197 (1999).
[21] S. Balay, K. Buschelman, W. D. Gropp, D. Kaushik, M. G. Knepley, L. C. McInnes, B. F. Smith, and H. Zhang, PETSc Library, http://www.mcs.anl.gov/petsc.
[22] V. Hernandez, J. E. Roman, and V. Vidal, ACM Trans. Math. Software **31**, 351 (2005); SLEPc Library, http://www.mcs.anl.gov/petsc.
[23] J. P. Karr and L. Hilico, J. Phys. B: At., Mol. Opt. Phys. **39**, 2095 (2006).
[24] M. Born and K. Huang, *Dynamical Theory of Crystal Lattices, Appendix VIII*, 1st ed. (Oxford University Press, London, 1954).
[25] G. Hunter, Int. J. Quantum Chem. **9**, 237 (1975).
[26] N. I. Gidopoulos and E. K. U. Gross, Philos. Trans. R. Soc., A **372**, 20130059 (2014).